Efficient Inductance Extraction via Windowing†

Michael Beattie and Lawrence Pileggi

Carnegie Mellon University
Department of Electrical and Computer Engineering
Pittsburgh, PA 15232, USA
beattie@ece.cmu.edu, pileggi@ece.cmu.edu

ABSTRACT

We propose a new, efficient and accurate localized inductance modeling technique via windowing in a manner that is analogous to localized capacitance extraction. The stability and accuracy of this process is made possible by twice inverting the localized inductance models, and in the process exploit properties of the magnetostatic interactions as modeled via the susceptance (inverse inductance). Application of these localized double–inverse inductance models to actual IC bus examples demonstrates the significant improvement in simulation efficiency and overall accuracy as compared to alternative methods of approximation and simplification.

I. INTRODUCTION

For modern digital ICs the logic path delays can be dominated by the influence of parasitic capacitive and inductive coupling among the metal interconnect wiring. As technologies push the performance to its limits, it is necessary to find increasingly more detailed interconnect models to predict the signal delay more accurately. The growing complexity of today's integrated systems, however, makes this computationally very expensive. Increasing system size makes efficient analyses of parasitics and performance imperative. Reconciling these two contradicting requirements is an extremely difficult task. Full three-dimensional interconnect models are generally of unmanageable size and density such that they are not useful for analysis and simulation purposes without additional approximations and simplifications.

Of particular focus is the modeling of on–chip inductance and its interactions with on–chip capacitance. While operating frequencies are making on–chip inductance evident, localizing the magnetic couplings for efficient extraction and analysis is challenging. Localized extraction techniques have been used with some success in the past for reducing the size of interconnect models. It has been demonstrated, however, that simple truncation — merely discarding long range couplings — can destroy the stability of the electromagnetic (EM) model. Shell models [4] have been applied successfully for stable localized extraction, but finding the correct shell sizes for a particular target accuracy is not straightforward.

† This work was supported by the MARCO/DARPA Gigascale Silicon Research Center (GSRC), the National Science Foundation, and a grant from Intel Corporation.

In this paper we propose a novel localized extraction technique for inductance modeling via windowing --- capture local interactions within small windows, then combine these localized models into a complete inductance matrix. This approach does not localize couplings in the inductance matrix directly, but begins with partial inductance models for small localized windows. These small, localized inductance matrices are inverted individually to generate the corresponding localized *susceptance matrices S*. As we will show in this paper, *S* has properties similar to the capacitance matrix, such as shielding, which can be exploited to combine the localized window models into a complete, *sparse*, susceptance matrix. We then invert this sparse susceptance matrix and produce a complete inductance matrix that we can further sparsify in an accurate and stable manner.

In [7] the direct use of the inverse of inductance for simulation has been suggested, but widespread commercial support for these models is not yet available.

II. WINDOWING FOR INDUCTANCE EXTRACTION

The inductance extraction flow we are proposing in this paper consists of the following steps:

- Generate a partial inductance matrix $L^{(j)}$ for active conductor *j* and all conductors within a window around it.
- Find the current flowing through these conductors for which the total flux for active conductor *j* through its loop with infinity is unity and for each other conductors in the window the total flux is zero. This produces the susceptive couplings $S^{(j)}_{ij}$ between active conductor *j* and the group of conductors within a window around it.
- Repeat these two previous steps for all conductors in turn as active conductors.
- Merge all $S^{(j)}_{ij}$ submatrices into one complete, sparse susceptance matrix that approximates the magnetic interactions for the entire interconnect system.
- The combined susceptance matrix will be asymmetric, since $S^{(j)}_{ij}$ is typically not equal to $S^{(i)}_{ij}$. By choosing the value with the *smaller magnitude* for both entries, we can prove that the complete susceptance model can be rendered symmetric and stable.

- Invert the sparse, symmetric susceptance matrix to generate an inductance matrix. The truncation in the susceptance domain makes this matrix much easier to sparsify than the original inductance model.

This double–inverse inductance matrix can then be used for timing analysis or simulation without loss of generality. We present examples of the efficacy of these models in Section V. But we will first begin by describing some important properties of capacitance and susceptance matrices which facilitates this extraction methodology.

III. Properties of EM Interaction Matrices

We assume a boundary element approach where the source (charge/current) density is constant for each section (panel/filament).

$$\psi_i^{\alpha} = (\phi_i\,;\, A_{i,x}\,;\, A_{i,y}\,;\, A_{i,z}) \tag{1}$$

is the vector of average potentials for section i. The field type α is 0 for the electrostatic and 1, 2 or 3 for the *xyz* magnetostatic cases. The *discrete* source vector is

$$\gamma_j^{\alpha} = (q_j/\varepsilon\,;\, \mu I_{j,x} l_{j,x}\,;\, \mu I_{j,y} l_{j,y}\,;\, \mu I_{j,z} l_{j,z}) \tag{2}$$

where q_j and $I_{j,\{xyz\}}$ are the charge and the three current components for this section. The $l_{j,\{xyz\}}$ are the dimensions of section j. We can write the discretized electromagnetic interconnect interactions as

$$\hat{\psi}^{\alpha} \approx K^{\alpha}\hat{\gamma}^{\alpha} \quad with$$
$$K_{ij}^{\alpha} \equiv \frac{1}{W_i^{\alpha}}\frac{1}{W_j^{\alpha}}\frac{1}{4\pi}\int_{W_i^{\alpha}}\int_{W_j^{\alpha}}\frac{1}{\|\vec{r}_i - \vec{r}_j\|}dW_i^{\alpha}\,dW_j^{\alpha} \tag{3}$$

by defining the matrices K^{α}. W_i^{α} is the content (panel area or filament volume) of section i for field type α. These in turn form the four diagonal blocks of the *electromagnetic interaction matrix K* in

$$\hat{\psi} \approx K\hat{\gamma} \tag{4}$$

where $\hat{\psi}$ and $\hat{\gamma}$ are formed by concatenating $\hat{\psi}^{\alpha}$ or $\hat{\gamma}^{\alpha}$.

The *capacitance matrix*, $C = S^0$, can be found by inverting the *potential matrix* $P = K^0$. The inverses of the *partial inductance matrices* $L_x = K^1$, $L_y = K^2$ and $L_z = K^3$ are the *susceptance matrices* S^1, S^2 and S^3 of the system. Together these four blocks form the *inverse interaction matrix S*.

• **Positive Definiteness of *K*:** The term $K\hat{\gamma}$ represents (within the accuracy of the discretization) the electric scalar and magnetic vector potential. The combined energy stored in the electromagnetic field is $(\int[\rho(\vec{r})\phi(\vec{r}) + \vec{j}(\vec{r})\cdot\vec{A}(\vec{r})])/2$, and must be non–negative (see [2][pg. 237]). In our matrix notation we then have

$$\hat{\gamma}^T K\hat{\gamma} \geq 0 \tag{5}$$

which is zero if and only if no electric and magnetic sources are present. It follows that K, as well as S, must be positive definite.

• **Diagonal Elements of *S* are positive:** K is positive definite, so we know

$$\forall\hat{\gamma} \neq \hat{0} \;:\; \hat{\gamma}^T K\hat{\gamma} > 0 \tag{6}$$

If we choose $\hat{\gamma}$ to be the solution of $K\hat{\gamma} = \boldsymbol{e_i}$ (which has to exist and be unique), where $\boldsymbol{e_i}$ is the unit vector with 1 as i^{th} element, then we have $\hat{\gamma} = S\boldsymbol{e_i}$ and with (6) find

$$\forall\boldsymbol{e_i} \;:\; \boldsymbol{e_i}^T S^T K S\boldsymbol{e_i} > 0 \tag{7}$$

With $SK = I$ we get

$$\forall\boldsymbol{e_i} \;:\; \boldsymbol{e_i}^T S^T\boldsymbol{e_i} \equiv S_{ii} > 0 \tag{8}$$

This equates to all diagonal elements of S being positive, since S is a square matrix.

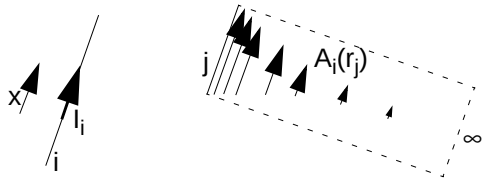

Fig. 1: Current in segment i in positive x–direction creates vector potential in j in positive x–direction as well. Compensating current in j must flow in negative x–direction.

• **Off–Diagonals of *S* are negative or zero:** Next we show that all off–diagonal elements of S must be either negative or zero. For the electric case ($\alpha = 0$) this is shown in [8][pg. 223]. If we have unit potential at conductor i and zero potential everywhere else, then (8) tells us that we will have a positive charge on conductor i. This positive charge will create a positive potential at the locations of all other conductors and negative charge needs to be added to all those grounded conductors to ensure zero potential. Thus, for $\alpha = 0$ (electric fields), we find that $\forall j \neq i \;:\; S_{ij}^0 < 0$.

For $\alpha = 1,2,3$, we have defined the currents to be directed in the positive *xyz* directions. So, similar to the electric case above, if we, for instance, require a unit vector potential along conductor i in x–direction, there must be, because of (8), a current flowing through conductor i in *positive* x–direction (see Fig. 1). This creates magnetic vector potential within the loops of the other segments j. To get a zero vector potential for all other segments j, currents in *negative* x–directions must flow through those segments. Similar for y

and z–directions. So the off–diagonal elements of S must be negative here as well (for the given current direction convention). So for the entire inverse interaction matrix we find

$$\forall j \neq i \;:\; S_{ij} < 0 \tag{9}$$

• **Diagonal Dominance of *S*:** Since sources $\hat{\Gamma}$ are only found on or within the conductors in the system, we find that the electrostatic and magnetostatic potentials in the insulator satisfy Laplace' equation with the surfaces of the conductors and infinity being the boundaries of the domain:

$$\nabla^2 \hat{\Psi} = \hat{0} \tag{10}$$

If we require the (electro– or magnetostatic) potential $\hat{\Psi}$ to be unity for all conductors, then each element of $\hat{\Psi}$ must be maximal on each conductor. This is a fundamental property of harmonic functions — solutions of Laplace' equation (see [9]). It follows that the gradient of each of the four elements of $\hat{\Psi}$ on the surface of each conductor must be pointing into the conductors. For the electric case this means all surfaces are positively charged, because the electric field points into the dielectric material everywhere.

For the magnetic case this means that the vector potential components A_x, A_y and A_z are positive everywhere, since solutions of Laplace' equation are maximal and minimal on the boundary of their definition domain. Here the maximum (by construction unity) are the combined conductor surfaces, the minimum is infinity where the vector potential is zero by convention. Finally, since the vector potential components are positive everywhere, currents must flow in the positive *xyz* directions in all the conductors as well, since if not, there would be locations with negative vector potential components, creating a contradiction.

So combining the electrostatic and magnetostatic case, we find

$$\hat{\gamma} = S\hat{\psi} = S\begin{bmatrix} 1 \\ \dots \\ 1 \end{bmatrix} > \hat{0} \text{ so for each row: } \sum_j S_{ij} > 0 \tag{11}$$

The 'greater as' in the first part of (11) acts element for element. With (8) and (9), which give the signs of the S_{ij} (diagonals positive, off–diagonals negative!), we find diagonal dominance for S:

$$|S_{ii}| > \sum_{j \neq i} |S_{ij}| \tag{12}$$

• **Positive Definiteness of Truncated *S*:** S was shown to be positive definite. Due to its diagonal dominance, the positive definiteness of S is preserved when off–diagonal elements are set to zero — a property not available for K. For this we use the following theorem from linear algebra [12][pg. 349] for a matrix A:

If all $A_{ii} > 0$ and A, A^T diagonal dominant
then A is positive definite. (13)

Diagonal dominance and positivity of the diagonal elements of S have been shown previously. With (13) the positive definiteness of the sparsified S follows.

• **Shielding Effect in *S*:** To assist in understanding the physical interpretation of susceptance, we ask: *What* is the significance of j^{th} column of S? The j^{th} column of S is the amount of source (charge or current) necessary *on* or *flowing through* the conductors to force conductor j to unit (electric or magnetic) potential and all other conductors to zero potential. An individual term S_{ij}, when i and j are far removed, must include shielding effects for the electrostatic *as well as* for the magnetostatic fields. The 'source necessary' in some conductor i to force it to zero potential already takes into account that some of the original field of the reference (unit potential) conductor j has been compensated by charges / currents on zero potential conductors closer to j. This in turn means that the magnitude of the elements in S_{ij} drops off much faster with distance between i and j. This enhances sparsification, since elements which are 'large enough' in S are easier to distinguish from those that are 'too small', thereby forming a much smaller set than for the interaction matrix K.

• **Stability of *S* under Window Inversion:** Since the shielding effect renders all but a few short–distance couplings negligible, the idea to exploit this to make the inversion from K to S more efficient by only including those few neighbors of the current unit potential conductor in the inversion. That is, the inversion is restricted to *extraction windows* around each conductor, thereby replacing the inversion of a huge, dense N x N matrix — N being the total number of conductors in the system — by N times an inversion of much smaller n_j x n_j matrices. This results in N individual, small matrices $S(j)$, where n_j is the number of conductors to which segment j has significant couplings.

The $S(j)$ are all diagonally dominant, since the proof above applies to each of the small conductor subsets individually. Clearly, for this approach the coupling $S_{ij}(j)$ need not be equal to $S_{ji}(i)$, since the set of 'significant neighbors' is usually different for different segments i and j. However, when we assemble our sparse S' matrix for the entire system from the individual $S(j)$, we need to ensure symmetry of S'. To guarantee positive definiteness of S', we choose

$$S'_{ij} = S'_{ji} = \max\{S_{ij}(j), S_{ji}(i)\} \tag{14}$$

Since we know that all off–diagonal elements of any inverse interaction matrix are non–positive, this means we select the element with the *smallest magnitude*. This ensures the diagonal dominance of S' when assembling it from elements of the $S(j)$, while preserving the largest degree of accuracy. With (13) we then find that the sparse approximation S' is positive definite.

IV. Double–Inverse Inductance Models

Two major drawbacks using partial inductance to model magnetic interactions for on–chip interconnect are: 1) the slow, logarithmic decay of the couplings with the distance between the filaments; and 2) the absence of any shielding effect. This makes localizing partial inductance difficult. In the previous section we have shown, however, that using susceptance rather than inductance for modeling the magnetic field interactions is much more beneficial. Using S directly in simulators and timing analysis tools as proposed in [7], however, is not readily supported by most programs available today.

We have shown in the last section that it is possible to ensure the stability of sparse susceptance matrices. We apply a windowing approach, solving many local inductance systems rather than one large problem. When assembling all partial results into a sparse global susceptance matrix, we have shown that the stability of the symmetric result is ensured by choosing the off–diagonal with the smaller magnitude.

The window size can be chosen to include only long–range susceptive couplings above a given magnitude threshold relative to the self terms. One percent cutoff means, for instance, that the window size was chosen such that increasing the window only added new susceptive couplings less than 1% of the self term for a given active conductor. The window sizes necessary are much smaller for susceptance than for the initial inductive model, due to the shielding effect for S.

The global, sparse susceptance matrix is then positive definite, as shown in Section III, so inverting this sparse S matrix back into an inductance representation, using sparse matrix solving techniques [10], yields again a positive definite matrix.

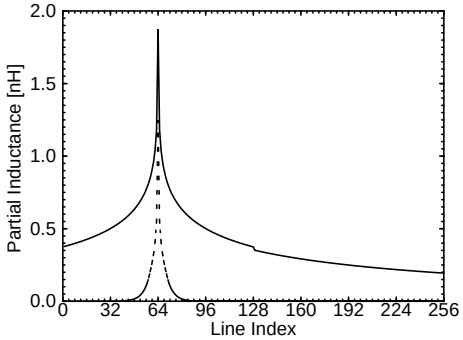

Fig. 2: Comparison of original inductive couplings with double–inverse L. Shown are couplings of all bus lines of example in Fig. 3 to line 64 (middle of first block). Solid line for original partial inductance, dotted line for double–inverse L (all elements of susceptance matrix smaller than 1 % of maximum were discarded).

The resulting double–inverted partial inductance matrix generally contains far fewer significant elements than the original inductance matrix, making further sparsification of L much easier (see Fig. 2). To preserve positive definiteness of the doubly inverted inductance matrix, we add the magnitude of off–diagonals which we cancel during sparsification to the corresponding diagonal elements. That this procedure preserves positive definiteness is easy to show. We define a symmetric matrix $M_{ij}(p,q)$ which is +1 for $i=j=p$, and $i=j=q$, either +1 or –1 for both ($i=p,j=q$) and ($i=q,j=p$), and 0 everywhere else.

$x^T M(p,q)x$ is always greater or equal to zero, which can be shown by explicitly calculating the expression. If a symmetric matrix A is positive definite, then the matrix $B=A+|A_{pq}|*M(p,q)$ must be positive definite as well. If we choose the sign of the off–diagonals in $M(p,q)$ opposite to the sign of A_{pq}, then $B_{pq}=B_{qp}=0$.

Since most of the off–diagonal terms of the double–inverse inductance matrix are very small (see Fig. 2), this procedure ensures the positive definiteness of the resulting sparse double–inverse inductance matrix while not significantly changing the diagonal elements. We use the same cutoff percentage threshold for the double–inverse inductance matrix as for the susceptance matrix.

This sparse inductance model can now efficiently and accurately represent magnetic interactions within interconnect without compromising stability. Examples will be presented in the following to demonstrate the efficacy of this approach.

V. Examples

A. Single Layer 2 x 128 Bit Bus

We demonstrate our inductance modeling method on a bus consisting of two blocks of 128 lines (W 1 µm, H 2 µm, Sp 1 µm, L 1000 µm) with 16 µm additional gap between the two blocks (see Fig. 3). The driver resistance R_{Dr} is 70 Ω and the load capacitance C_{Ld} is 2 fF. Every sixteenth line is a return line (no driver resistance).

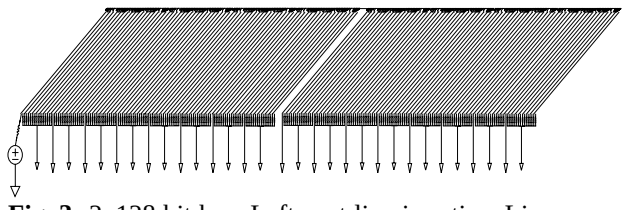

Fig. 3: 2x128 bit bus. Leftmost line is active. Line numbering from left to right.

In Fig. 4 the far end node voltage responses for two lines of the structure are shown for 1V step and 10 ps ramp inputs. As expected, the far end response reduces in magnitude with increasing distance from the active line. The refer-

ence results (white circles) are obtained by including all individual couplings, leading to high runtimes and memory consumption (see Table 1). Double–inverse inductance models are sparsified as described in Section IV dependent on cutoff percentage (the smaller, the more accurate). For simple truncation we merely set to zero all off–diagonals which are zero for the double–inverse with the given cutoff threshold to ensure fair comparison of the efficiency and accuracy of the different methods.

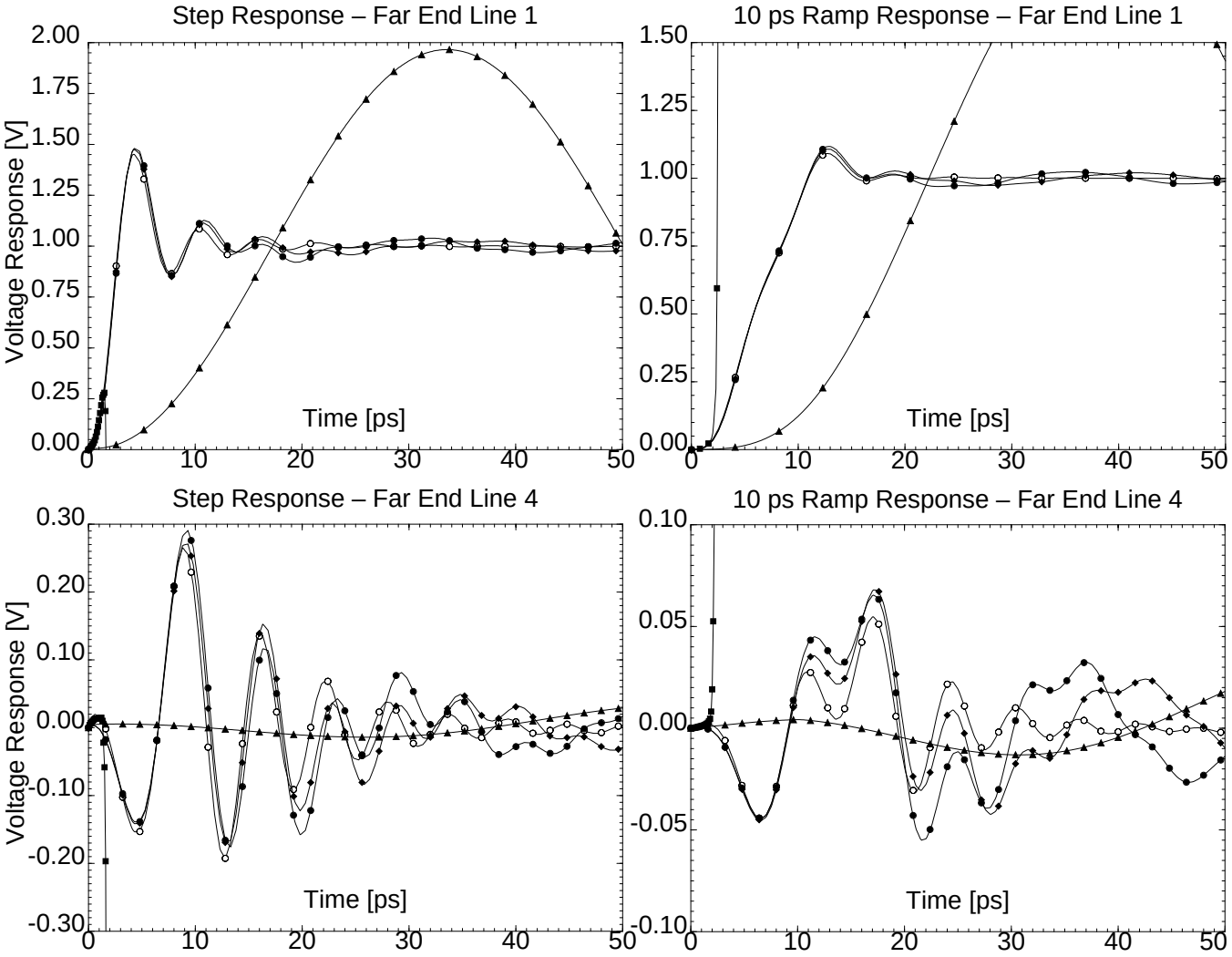

Fig. 4: Voltage responses at far ends of lines 1 and 4 of 2x128 bit bus. Curves with ○ are reference results for full L and C matrices. Approximations: Double–inverse inductance with cutoff 1% (●); double–inverse L with cutoff 0.5% (◆); simple truncation cutoff 1% (■); stabilized simple truncation cutoff 1% (▲).

The waveforms for our double–inverse inductance localization method are very close to the corresponding reference results, and especially the time interval containing the first few minima and maxima is captured very well by the double–inverse approximation leading to very high accuracy for interconnect timing analysis. The runtime and memory requirements, however, are significantly smaller than for the reference case. Speedup factors are shown in Table 1.

It should be noted that the double–inverse inductance model is effective at higher frequencies, which is where inductive effects have the most impact and predominantly determine the ringing and overshoot for timing analysis. For lower frequencies the damping of double inverse is less, therefore a low–amplitude, low–frequency oscillation around steady state remains while ringing is damped much quicker for the reference result. Overall, our double–inverse inductance model shows excellent agreement with the exact result.

For comparison we also tried to generate a corresponding waveform using simple truncation on the original partial

inductance. However, this creates an ill–conditioned inductance model which leads to diverging waveforms. A more extensive study of this is available in [4]. This is observed in the results in Fig. 4 (squares) which coincide with the reference solution for about the first picosecond of simulation time, then diverge towards positive or negative infinity.

Symbols see Fig. 4:	○	●	◆	■	▲
Runtime (step) [s]	17550	38	87	680	32
Speedup Factor (step)	1.0	460	200	26	550
Runtime (ramp) [s]	20050	41	87	530	30
Speedup Factor (ramp)	1.0	490	230	38	670
Memory [MByte]	112800	5760	10040	14510	5760
Capacitance El.	32481	3280	4823	3280	3280
Inductance El.	32896	4201	6392	4201	4201
Sparsity [%]	0.0	88.5	82.8	88.5	88.5
HSpice internal El.	65890	7994	11728	19190	7994

Table 1: Simulation cost comparison for 2x128 bit bus example in Fig. 3.

It is possible to avoid this stability problem by simply adding the truncated mutual partial inductances to the self term, much as described for our double–inverse inductance model in Section IV. However, since the off–diagonal terms are *significant in magnitude* for the partial L matrix during simple truncation, this will grossly overestimate the magnetic self coupling leading to much lower response waveform frequencies and very low accuracy (triangles in Fig. 4).

B. Three Layer Bus Structure

Our second example consists of three parallel bus structures with the leftmost wire of the middle layer being active. All wires are 1000 µm long (cross–section in Fig. 5). Layer 1: W 1 µm, H 2 µm, Sp 1 µm, R_{Dr} 70 Ω, C_{Ld} 2 fF. Layer 2: W 3 µm, H 2 µm, Sp 1 µm, R_{Dr} 50 Ω, C_{Ld} 2 fF. Layer 3: W 6 µm, H 3 µm, Sp 2 µm, R_{Dr} 25 Ω, C_{Ld} 2 fF. Every eighth line is a return line.

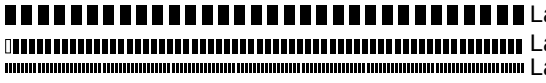

Fig. 5: Three Layer Bus Example. 128 bit on layer 1, 64 on layer 2 and 32 bit on layer 3. Active line shown white.

The clear advantage of our double–inverse model over the simple truncation approach is also evident in the results for this example, shown here in Fig. 6. Our observations from the previous example apply in this case as well.

The presence of interconnect above and below the layer in which the active line is placed increases the number of wires to which coupling is significant for accurate simulation. Therefore, for the same cutoff threshold values, the sparsity of the approximate models is lower as for the single layer example. However, since the total number of conductors is smaller than for the 2x128 bit bus example, the runtimes and memory consumption are smaller as well.

Due to the higher density of surrounding conductors for each wire and the resulting lower sparsity of the inductance approximations, the speedup across the board is lower than for the previous example, but still quite significant.

Symbols see Fig. 6:	○	●	◆	■	▲
Runtime (step) [s]	9390	72	310	1700	43
Speedup Factor (step)	1.0	130	30	5.5	220
Runtime (ramp) [s]	8950	75	310	1790	45
Speedup Factor (ramp)	1.0	120	29	5.0	200
Memory [MByte]	87230	7650	16070	29150	7650
Capacitance El.	25424	3125	4662	3125	3125
Inductance El.	25200	6962	12459	6962	6962
Sparsity [%]	0.0	80.0	66.1	80.0	80.0
HSpice internal El.	51073	10536	17570	27620	10536

Table 2: Simulation cost comparison for three layer bus example in Fig. 5.

VI. Conclusions and Future Directions

We have presented a novel and accurate windowing technique for inductance extraction. This approach provides for sparsification of the inductance matrix in a manner that is more robust and accurate as compared with other simplification schemes. It is also shown to preserve model stability while avoiding high memory consumption and runtimes. This localization process requires efficient inversion of the small L and S submatrices that correspond to the applied windows.

Although this inductance localization approach provides for a substantial improvement over existing methods, neglecting long distance couplings or merging them into short distance couplings will always limit the modeling accuracy. To efficiently create accuracy beyond the level which can be provided by localized extraction requires *hierarchical models*. Efficient extraction of a hierarchical susceptance and double–inverse inductance model appears to be viable using existing hierarchical extraction approaches [5]. To integrate these hierarchical models into circuit netlists will be the focus of future research.

References

[1] A. Ruehli, *Inductance Calculations in a Complex Integrated Circuit Environment*, IBM J. Res. Dev., **16**, No.5 (September 1972).

[2] J. Jackson, *Classical Electrodynamics*, 2nd Ed., John Wiley & Sons, New York (1975).

[3] E. Rosa, *The Self and Mutual Inductance of Linear Conductors*, Bul. Nat. Bureau of Standards, **4** (1908).

[4] M. Beattie, L. Pileggi, *IC Analyses Including Extracted Inductance Models*, 36th DAC (June 1999).

[5] M. Beattie, L. Pileggi, *Electromagnetic Parasitic Extraction via a Multipole Method with Hierarchical Refinement*, Proc. ICCAD 1999 (November 1999).

[6] L. Nagel, R. Rohrer, *Computer Analysis of Nonlinear circuits, Excluding Radiation (CANCER)*, IEEE J. Solid State Circ., **SC–6**, pp. 162–182 (August 1971).

[7] A. Devgan, H. Ji, W. Dai, *How to Efficiently Capture On–Chip Inductance Effect: Introducing a New Circuit Element K*, Proc. ICCAD 2000 (November 2000).

[8] D. Ling, A. Ruehli, *Interconnection Modeling*, in: *Circuit Analysis, Simulation and Design*, Elsevier Science Publishers B.V., North–Holland, (1987).

[9] I. Bronshtein, K. Semendyayev, *Handbook of Mathematics*, Third Edition, Van Nostrand Reinhold.

[10] G. Golub, C. Van Loan, *Matrix Computations*, 3rd Ed., Johns Hopkins University Press, Baltimore (1996).

[11] W. Press, S. Teukolsky, W. Vetterling, B. Flannery, *Numerical Recipes in C*, 2nd edition, Cambridge University Press, New York (1992).

[12] R. Horn, C. Johnson, *Matrix Analysis*, Cambridge University Press, Cambridge (1985).

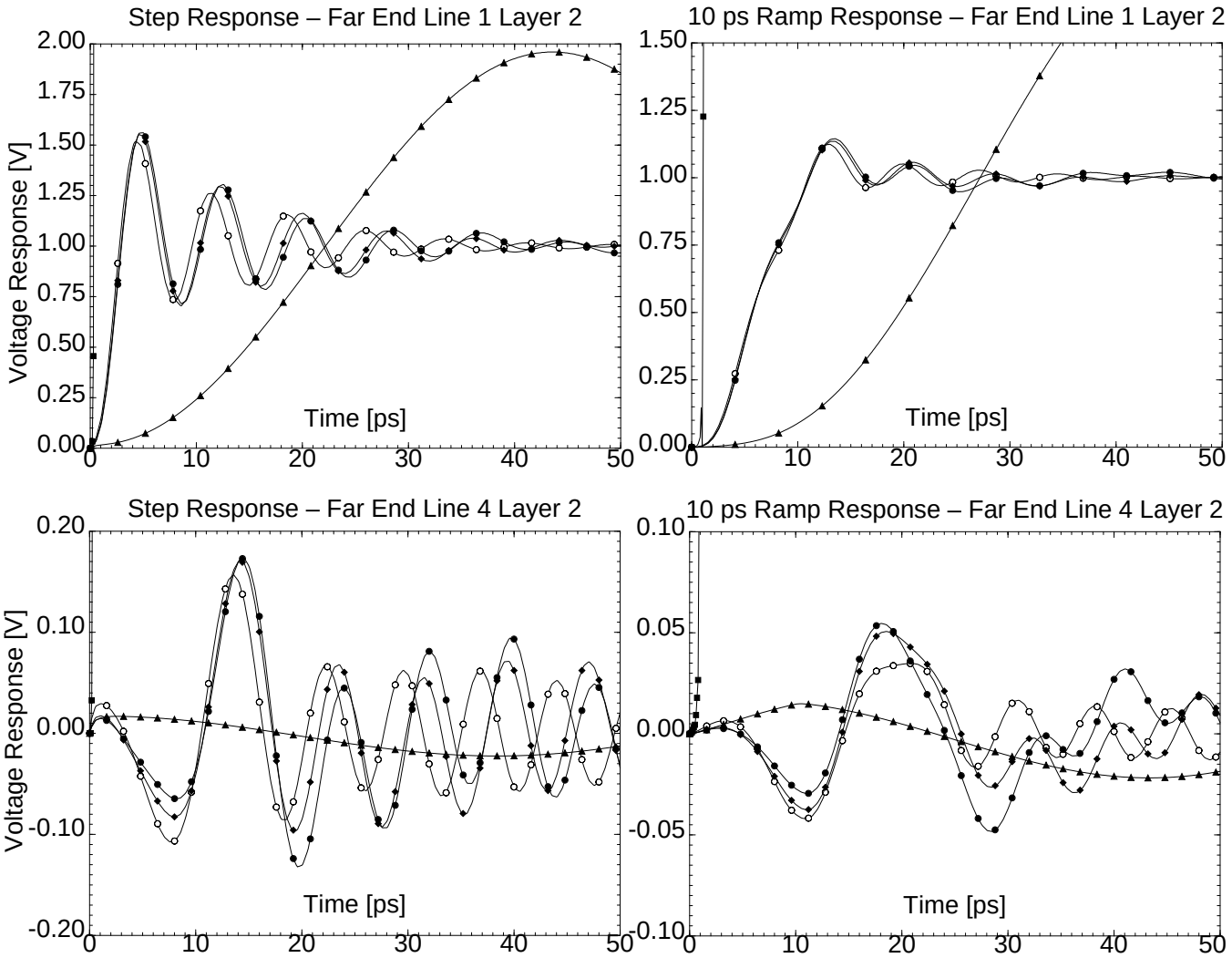

Fig. 6: Voltage responses at far ends of lines 1 and 4 from the left in the middle layer of Fig. 5. Curves with ○ are reference results for full L and C matrices. Approximations: Double–inverse inductance with cutoff 1% (●); double–inverse L with cutoff 0.5% (◆); simple truncation cutoff 1% (■); stabilized simple truncation cutoff 1% (▲).